Efficient *in vivo* Vascularization of Tissue Engineering Scaffolds

Anja Hegen[1,*], **Anna Blois**[1,*], **Crina E. Tiron**[1], **Monica Hellesøy**[1], **David R. Micklem**[1], **Jacques E. Nör**[4], **Lars A. Akslen**[2,3], and **James B. Lorens**[1,5]

[1] Department Biomedicine, University of Bergen, N-5009, Bergen, Norway

[2] The Gade Institute, Section for Pathology, University of Bergen, N-5009, Bergen, Norway

[3] Department of Pathology, Haukeland University Hospital, N-5021, Bergen, Norway

[4] School of Dentistry and Department of Otolaryngology, University of Michigan, Ann Arbor, MI, 48109-1078

Abstract

The success of tissue engineering depends on the rapid and efficient formation of a functional blood vasculature. Adult blood vessels comprise endothelial cells and peri-vascular mural cells that assemble into patent tubules ensheathed by a basement membrane during angiogenesis. Using individual vessel components, we characterized intra-scaffold microvessel self-assembly efficiency in a physiological *in vivo* tissue engineering implant context. Primary human microvascular endothelial- and vascular smooth muscle cells were seeded at different ratios in poly-L lactic acid (PLLA) scaffolds enriched with basement membrane proteins (Matrigel) and implanted subcutaneously into immunocompromised mice. Temporal intra-scaffold microvessel formation, anastomosis and perfusion were monitored by immunohistochemical, flow cytometric and *in vivo* multiphoton fluorescence microscopy analysis. Vascularization in the tissue engineering context was strongly enhanced in the implants seeded with a complete complement of blood vessel components: Human microvascular endothelial and vascular smooth muscle cells *in vivo* assembled a patent microvasculature within Matrigel-enriched PLLA scaffolds that anastomosed with the host circulation during the first week of implantation. Multiphoton fluorescence angiographic analysis of the intra-scaffold microcirculation showed a uniform, branched microvascular network. 3-D image reconstruction analysis of hPASMC distribution within vascularized implants was non-random and displayed a preferential peri-vascular localization. Hence, efficient microvessel self-assembly, anastomosis and establishment of a functional microvasculture in the native hypoxic *in vivo* tissue engineering context is promoted by providing a complete set of vascular components.

Keywords

angiogenesis; scaffold; endothelial; mural cell; microcirculation; multiphoton

1. Introduction

Tissue engineering endeavours to replace and restore organ function to treat end-stage disease. The success of tissue engineering strategies depends on the efficient formation of a functional blood vasculature to serve the metabolic needs of bioengineered tissues.

[5]To whom correspondence should be addressed: James B. Lorens, Ph.D., Department of Biomedicine, University of Bergen, Jonas Lies vei 91, N-5009 Bergen, Norway, Telephone: +47 55 58 67 76, Fax: ++47 55 58 63 60, jim.lorens@biomed.uib.no.
*These authors contributed equivalently

However, contemporary tissue engineering approaches are hampered by inadequate vascularization of the hypoxic engineered microenviroment that debilitates tissue development (Muschler et al., 2004, Patterson et al., 2008). Inclusion of angiogenesis stimulating factors can improve scaffold vascularization, however this process is slow and difficult to control (Lazarous et al., 1996) Formation of new blood vessels requires cell-cell and cell-matrix interactions between blood vessel components; endothelial cells mural cells (vascular smooth muscle cells, pericytes) and vascular basement membrane that collectively regulate vessel assembly (Black et al., 1998, Black et al., 1999, Nguyen and D'Amore, 2001). Mural cells define a context comprising heterotypic cell-cell contact, extracellular matrix deposition and soluble factors that inhibit endothelial proliferation, maintain capillary diameter, regulate blood flow and provide survival signals for the cells in the blood vessel (Hall, 2006, Kutcher and Herman, 2009). Heterotypic cell-cell contacts at interdigitations between endothelial cells and mural cells provide a unique presentation context for paracrine factors such as VEGF and angiopoietins, which regulate endothelial cell responses (Darland and D'Amore, 1999). Hence, the generation of tissue-engineered microvascular networks in three- dimensional (3D) matrices utilizing only vessel-derived endothelial cells (EC) or EC differentiated from progenitor cell populations, will depend on the recruitment of host-derived mural cells such as vascular smooth muscle cells (SMC) for proper vessel maturation (Kaully et al., 2009). Studies with implanted endothelial spheroids demonstrated that the investment of engineered vessels by host mural cells enhances their stability (Alajati et al., 2008, Wenger et al., 2005). Alternatively, ectopic expression of anti-apoptotic genes such as Bcl-2 in microvascular endothelial cells can improve endothelial survival and microvessel stability *in vivo* (Schechner et al., 2000). ECs were shown to form functional microvessels when co-seeded with mouse mesenchymal cells in fibronectin–collagen type I protein gels (Koike et al., 2004). A functional blood vessel correlates with the transition of a growing vascular network to a quiescent vascular phenotype (Adams and Alitalo, 2007). Our laboratory has previously employed an *in vitro* organotypic vessel co-culture system in order to model vessel maturation (Evensen et al., 2009). Endothelial cells co-cultured with mural cells (SMC or mesenchymal stem cells) result in a spontaneous endothelial capillary-like network formation and deposition of a complex basement membrane leading to an endothelial VEGF-independent phenotype. We applied the principles defined by these *in vitro* results to address whether uniform vessel assembly can be accelerated in a physiological *in vivo* tissue engineering context (Nor et al., 2001). Our results emphasize the dominant pro-maturation effect of vascular smooth muscle cells that enforces formation of a uniform, branched functional intra-scaffold microvasculature, providing a methodological and conceptual basis for improving tissue engineering strategies.

2. Materials and Methods

2.1. Cells

Human Dermal Microvascular Endothelial Cells (HMVEC, single donor lot; Lonza) were grown in EGM-2 MV medium (Lonza). Human Pulmonary artery Smooth Muscle Cells (hPASMC, single donor lot; Lonza) were grown in SmGm medium (Lonza). Primary cells were used between passage 3–7. Phoenix A retroviral packaging cells (ATCC) were grown in Dulbecco's Modified Eagle Medium (DMEM) (4500 mg/ml glucose) (Sigma Aldrich) supplemented with 10% FBS (Euro Clone/PAA), 5% Penicillin/Streptomycin (Sigma Aldrich) and 5% L-Glutamine (Sigma Aldrich).

2.2 Retroviral transduction

Phoenix A retroviral packaging cells were transfected with GFP or RFP retroviral vectors (Evensen et al., 2009) as per Swift *et al* (Swift et al., 1999). Briefly, subconfluent Phoenix A were transfected by $CaCl_2$-precipitation in the presence of chloroquine (Sigma Aldrich).

Virus was harvested in EGM-2 MV or SmGm medium 48 hours post transfection and added to subconfluent HMVEC or hPASMC (passage 3–5) with 5 μg/ml protamine sulfate (Sigma Aldrich) for 16 hours. Transduced GFP-expressing HMVEC and RFP-expressing hPASMC were purified by flow cytometric sorting on a FACSAria Cell Sorter (BD Biosciences).

2.3 In vitro organotypic blood vessel system

A microtiter plate format *in vitro* organotypic blood vessel system assay was conducted as described (Evensen et al., 2009). Briefly, 6 000 GFP-expressing HMVEC and 50 000 hPASMC cells were co-seeded in EGM-2MV medium in a 96-well plate. Co-cultures were imaged after 72 hours using a fully automated high throughput fluorescence microscope (BD Pathway 855).

2.4. Experimental animals

For all experiments, non-obese mice with severe combined immunodeficiency disease (NOD/SCID) (Gade Institute/Taconic Farms) were used. The animals were approximately 6–8 weeks of age at the time of scaffold implantation. All experiments were approved by the Norwegian Animal Research Authority, and conducted according to the European Convention for the Protection of Vertebrates Used for Scientific Purposes.

2.5. Scaffold preparation

Poly-L Lactic Acid (PLLA) scaffolds were produced by a solvent-casting particulate-leaching technique, previously described by Nor *et al* (Nor et al., 2001) One gram of PLLA (Resomer L 206 S, Boehringer Ingelheim) was dissolved in 20 ml chloroform (Sigma) to yield a 5% solution. NaCl (Fisher scientific) was sieved trough a test sieve (Retsch) with a pore size of 450μm, and 3,45 g of the sieved NaCl was distributed in silanised glass beakers. The NaCl was mixed with the 5% PLLA solution, and the solvent was left to evaporate. Thereafter, the scaffolds were leached for 48 h with ddH_2O to wash out the NaCl, and then dried and cut into 6×6×1 mm pieces. Scaffolds were sterilized in a descending alcohol row from 100-70% EtOH, and kept in sterile PBS until implantation.

2.6. Tissue engineering model

Prior to implantation, scaffolds were dried briefly on sterile paper and filled with a total of 1×10^6 cells in 36 μl of 50:50 EGM-2 MV and growth factor reduced phenol red-free Matrigel (BD). The scaffolds were left at 37 °C for 30 min, for the Matrigel to solidify. Scaffolds were seeded with 1×10^6 HMVEC alone, 1:1 (500 000 HMVEC: 500 000 hPASMC) or 1:4 (200 000 HMVEC: 800 000 hPASMC) ratios. For each experimental group, 5 mice were implanted with two scaffolds each. Acellular scaffolds containing Matrigel only were implanted into 4 mice; and scaffolds seeded with 1×10^6 hPASMC only were implanted into 5 mice, to provide negative controls for histology and imaging.

NOD/SCID mice were anesthetized with an intramuscular injection of 20μl 1:2 concentration of Rompun (Xylazin) (20mg/ml) (Bayer Health Care) and Narketan (Ketamin) (100mg/ml) (Vétoquinol) in the thigh muscle. A 2.5 cm incision was made on the back of the mouse, and scaffolds were placed in skin flaps at the flanks. After 7, 14 or 21 days, the mice were sacrificed by cervical dislocation after deep Isoflurane (Schering-Plough) anesthesia, and scaffolds were recovered for fixation.

2.7. Histological staining

Scaffolds were fixed in 10% paraformaldehyde (PFA), and subsequently embedded for paraffin sectioning. Sections from the middle part of the scaffold were deparaffinized and stained with monoclonal mouse-anti human CD31 (M0823, DAKO), and monoclonal mouse

anti-human smooth muscle actin ((M0851, DAKO), visualized with 3,3′-diaminobenzidine tetrahydrochloride (DAB) (EnVision™ detection system, K5007, DAKO) and counterstained with Hematoxylin (DakoREAL™ Hematoxylin, S2020, DAKO). Antibody specificity was validated using sections from acellular and hPASMC only implants.

2.8. Functional multiphoton fluorescence microscopy analysis

In order to specifically label perfused human endothelial cells in the scaffolds, 200 μl of UEA-1 Lectin-FITC (Sigma-Aldrich) (1 mg/ml in sterile 0.9% NaCl) was injected into the lateral tail vein 30 min before sacrifice (Holland et al., 2005) Scaffolds were excised and immediately imaged using a Multiphoton Microscope (Leica SP5). Acquired serial images were analyzed using 3D image analysis software (IMARIS 6.3).

2.9. Flow cytometry analysis

Scaffolds were removed 30 min after injection with UEA-1 Lectin-FITC and homogenized using a syringe in a collagenase A solution (Sigma-Aldrich) (22U/ml). Cells were centrifuged at 1000 rpm for 5 minutes, washed with PBS and filtered with a 40 μm pore size filter. Cells were then washed one more time, resuspended in PBS and analysed by flow cytometry for FITC fluorescence. Propidium iodide staining (1 μg/ml, Molecular Probes) was performed in order to exclude dead cells from the analysis.

2.10. Image analysis

To quantify the number of vessels per mm^2 and the vessel diameter, histological sections of scaffolds were examined with a light microscope (Leica). Using the image processing program AnalySIS, the outlines of anti-hCD31-staining vessels in five fields of view of a section were encircled manually at 200 × magnification. The number of vessels from five fields of view was used to calculate the vessel diameter and number of vessels per mm^2. Vessels were subdivided into 5 categories based on diameter: <10 μm, 10–20, 20–30, 30–50 and 50μm that are characteristic for capillary arteriole, artery and immature vessels (Silverthorn et al., 2004).

Serial multiphoton fluorescence images acquired from *ex vivo* scaffolds were reconstructed using 3D-image analysis software (IMARIS 6.3). The length and the diameter of UEA-lectin-FITC stained vessels was quantified in images using IMARIS. Analysis of the mean distance between human UEA-lectin-FITC stained vessels and RFP-expressing hPASMC in the scaffolds was performed as follows: Binary masks of voxels identified as belonging to vessels or smooth muscle cells (green and red in Figure 7A) were exported from IMARIS 6.3 as a series of TIFF images and imported as image stacks into the Fiji distribution of ImageJ (Rasband, 1997–2008). The distance of every voxel to the nearest hPASMC/RFP was calculated by applying the Euclidean Distance Transformation to the hPASMC/RFP image stack (Local Thickness plugin, Computing Local Thickness of 3D Structures with ImageJ," R.P. Dougherty and K-H Kunzelmann, Microscopy & Microanalysis 2007 Meeting August 5–9, 2007, Ft. Lauderdale, Florida (www.optinav.com/LocalThicknessEd.pdf). The distances for the subset of voxels forming the surface of the vessels was obtained by applying the Binary Outline tool to the HMVEC/UEA-1-lectin-FITC image stack, and using this to mask the Euclidean distance map calculated above. This yielded the distance of each of 159147 voxels on the vessel surfaces to the nearest hPASMC/RFP voxel.

2.11. Statistics

Statistical significance of the data was evaluated using a one-tailed Student's t-test. Statistically significant differences are denoted * ($p < 0.05$) or ** ($p < 0.01$). Number (n) in

each experiment refers to the number of scaffolds analyzed. This number was always 6 or larger (maximum n=12) for the immunohistochemistry analysis (SEM). For the *ex vivo* imaging n=4. All values in bar diagrams are presented as mean ± standard error of mean.

3. Results

3.1. Engineering mature human microvasculature from vascular components *in vivo*

Maturation of nascent blood vessels requires heterotypic vascular cell-cell interactions (Evensen et al., 2009). We analyzed a microtiter plate-format *in vitro* organotypic blood vessel system, comprising primary human dermal microvascular cells (HMVEC) co-cultured *in vitro* with human pulmonary artery-derived vascular smooth muscle cells (hPASMC). HMVEC-hPASMC co-cultures form extensive capillary-like networks and deposit a peri-endothelial basement membrane-like structure comprising vascular collagens (Fig. 1A–C). To determine if this vessel self-assembly process can form a functional microvasculature in an *in vivo* tissue engineering context we developed a tissue engineering model comprising HMVEC and hPASMC co-seeded with soluble basement membrane proteins (Matrigel) into a PLLA scaffold that is implanted into the dorsal subcutaneous tissue of an immunodeficient mouse host context (Nor et al., 2001). Subcutaneous PLLA scaffold implants become enveloped by connective tissue within 5 days and anastomose with local host fascial vessels (Nor et al., 2001). The subcutaneous microenviroment is hypoxic and thus is a relevant assessment of microvessel formation efficiency within a tissue engineering scaffold (Patterson et al., 2008).

PLLA scaffolds were fabricated with ≥ 450 μm pores and seeded with primary human vascular cells and soluble basement membrane proteins (Fig 2A–B). Primary human vascular cells attached to the PLLA scaffold surface within 24 hours (Fig 2C). PLLA scaffolds seeded with HUMVEC in monoculture or HUMVEC and vSMC at a 1:1 or 1:4 ratio, were implanted subcutaneously into immunocompromised NOD-SCID mice. Implants were retrieved 7, 14 or 21 days post-implantation and evaluated for the presence of intra-scaffold human microvasculature by immunohistochemistry using anti-human CD31 (Fig 3). Patent vessels stained by anti-human CD31 were evident throughout scaffolds seeded with the complete complement of vascular components 7 days after implantation (Fig. 3A). The presence of intralumenal red blood cells within the engineered human microvessels evidenced successful anastomosis with the local fascial vasculature and perfusion by the host circulation (Fig 3A). The intra-scaffold human vasculature was predominately functional at 14 and 21 days, displaying more uniform diameters and intralumenal host-derived red blood cells (Fig. 3B–C). No anti-human CD31-staining vessels were detected in sections from acellular or hPASMC only scaffold implants (Supplementary Fig. 1).

To ascertain the localization of the co-seeded hPaSMC, we conducted immunohistochemical analysis with anti-α-SMC actin (α-SMA) and anti-human CD31 in co-culture experiments with a 1:4 ratio of HMVECs to hPaSMCs. Tissue sections derived from 7-day and 14-day scaffold implants showed that anti-α-SMA staining cells co-localized with patent human CD31-staining vessels, likely representing co-seeded hPASMC as these timepoints precede the invasion of host mural-derived cells (Fig. 4A–B) (Nor et al., 2001). The anti-α-SMA staining cells became preferentially perivascular, encircling all scaffold human vessels at 14 and 21 days post-implantation (Fig 4B–C). Hence, co-seeded HMVEC and hPASMC adopt a native vessel configuration in the *in vivo* tissue engineering context.

3.2. hPASMC enhance the formation of small diameter microvessels in tissue engineering scaffolds

To determine if vessel self-assembly in the *in vivo* tissue engineering context enhanced the formation of small caliber microvessels by the presence of hPASMC, we co-seeded HMVEC and hPASMC at different ratios (1:1, 1:4), or HMVEC alone (1:0) into Matrigel-enriched PLLA scaffolds and evaluated vascularization parameters following subcutaneous implantation. Subcutaneous vascular cell implants were retrieved at different timepoints from the immunodeficient host mice and immunohistochemical morphometric analysis was conducted to measure the human intra-scaffold microvessel number and diameter. Microvessels were assigned to five categories based on the expected diameter distribution of the microvasculature (Gray H, 2004, Jenkins GW, 2007): <10 μm, 10–20 μm, 20–30 μm, 30–50 μm and >50 μm, where vessels >50 μm were defined as immature vessels, and vessels <10 μm and 10–20 μm were defined as a mature microvasculature. Remaining size groups were defined as transitional. Analysis of 7-day scaffolds showed that the vessels were mainly between 30–50 μm in diameter in all three vascular implants, indicative of maturing, transitional microvasculature (Fig. 5A). At 14 days post-implantation, the intra-scaffold microvasculature formed from the complete sets of vascular components showed a strong shift in the vessel size distribution to predominately 10–20 μm diameter microvessels, indicative of vessel maturation (Fig. 5B). The co-seeded HMVEC-hPASMC (1:4) group showed an increased proportion of <10 μm diameter microvessels, demonstrating a greater degree of capillary-caliber vessels (Fig. 5B). This microvessel distribution remained unchanged in the third week (Fig. 5C) for co-seeded implants. In contrast, implants lacking hPASMC did not show a commensurate microvessel size distribution shift until 21 days post-implantation, corresponding to the invasion of host mural cells (Nor et al., 2001). Notably, the efficiency of intra-scaffold microvascular formation (microvascular density per seeded EC) in the HMVEC-hPASMC (1:1 and 1:4) co-seeded scaffolds was enhanced 2.5- and 4-fold relative to HMVEC alone at day 14 (Fig. 5D). This is somewhat reduced at day 21, likely reflecting perfusion-mediated vascular remodeling. Collectively, these results indicate that a complete complement of vascular components stimulates the rapid formation and maturation of uniform small caliber microvessels in a tissue engineering context *in vivo*.

3.3 Analysis of tissue engineered functional microvasculature by fluorescence angiography

In order to functionally evaluate the intra-scaffold microcirculation engineered with the complete complement of vascular components, we conducted a fluorescence angiography analysis. UEA-1 lectin conjugated to FITC, which binds specifically to mannose moieties on the luminal surface of human endothelial cells, was injected into the host mouse circulation 30 minutes prior to sacrifice. To determine the presence of UEA-1-lectin-FITC stained HMVEC that manifest an intra-scaffold microcirculation, we interrogated cells harvested from excised 14-day scaffolds by flow cytometry. A large population of UEA-1-lectin-FITC stained cells were apparent in the green fluorescence channel. These perfused human endothelial cells exhibited high forward light scatter values, indicating that larger, potentially elongated endothelial cells comprise the functional microvasculature (Fig. 6A–B) (Ohnuma et al., 2006). In order to further investigate the morphology of perfused vessels, we conducted a morphometric analysis of the UEA-1 lectin-FITC stained human vessels in scaffolds by multiphoton fluorescence microscopy. A series of fluorescence images were collected from 100 μm inside vascularized scaffolds and reassembled by 3D image analysis to determine the length and diameter of individual vessel branches of the functional microvasculature. This UEA-lectin-FITC angiography analysis revealed the presence of an extensive branched network of perfused human microvessels within scaffolds implanted for 14 days (Fig 6C). No UEA-lectin-FITC-staining was detectable within 14-day acellular scaffolds or peripheral mouse fascial vessels (Supplementary Fig. 1). The UEA-lectin-FITC-

stained human endothelial cells displayed abundant filapodia consistent with ongoing vessel remodeling. The perfused human vessels were measured to be predominately <20μm in diameter, in accordance with the immunohistochemistry analysis (Fig 6D; Fig 5). Hence, tissue engineering implants comprising a complete complement of vascular components effectively self-assemble into a functional intra-scaffold microvasculature that establishes a microcirculation with the host.

In order to compare the location of the hPASMC relative to the perfused microvessels within the scaffold, we studied scaffolds seeded with HMVEC and RFP-expressing hPASMC (hPASMC/RFP). After two weeks, mice carrying HMVEC-hPASMC/RFP seeded scaffolds were injected with UEA-lectin-FITC. Following excision, scaffolds were analyzed for the presence of RFP-expressing hPASMC and UEA-lectin-FITC stained human endothelial cells by multiphoton fluorescence microscopy at 100 μm depths. 3D image reconstruction from multiphoton microscopy 3D-image stacks revealed that the majority of the hPASMC/RFP are located near the perfused endothelial cells (Fig. 7A–B). To quantitate this, volumetric pixel analysis of the 3D-image stacks was performed. The analysis showed that the hPASMC cells were closer to the perfused endothelial cells than would be expected for a random distribution, indicating co-localization. (Fig. 7C). hPASMC/RFP and UEA-1-lectin-FITC voxels within multiphoton microscopy 3D-image stacks were separated by a mean distance of 22.6 ± 14.6 μm versus an expected random distribution mean of 43.1 ± 0.07μm ($p \ll 0.0001$). This is consistent with the notion that hPASMC enhance vessel maturation in the tissue engineering context by juxtapositional heterotypic cell-cell interactions and paracrine signaling.

4. Discussion

A current challenge facing tissue engineering approaches is the expedient establishment of a microcirculation to meet the metabolic needs of the developing tissue implants and avoid cell death. We demonstrate here that efficient self-assembly of a functional microvasculature can be achieved in a physiological *in vivo* tissue engineering implant by providing individual vascular cellular and basement membrane components. In particular, our results emphasize the critical role of vascular mural cells in enforcing generation of a uniform, branched functional microvasculature in a tissue engineering context.

The recruitment of mural cells to the abluminal surface of nascent blood vessels is a key prerequisite for vessel maturation (Jain, 2003). Mural cells define a context comprising heterotypic cell-cell, cell-ECM deposition contacts and juxtacrine growth factor receptor signaling that regulate endothelial cell proliferation and survival (Adams and Alitalo, 2007, Beck and D'Amore, 1997, Carmeliet, 2003, Darland and D'Amore, 2001, Gaengel et al., 2009, Hellstrom et al., 2001, Jain, 2003, Korff et al., 2001). Proper growth factor receptor crosstalk between EC-mural cells also engenders local vascular basement membrane deposition required for vessel maturation and stability (Davis and Senger, 2005). This peri-vascular microenviroment serves an important role in delimiting endothelial responses to pro-angiogeneic factors emanating from the local tissue (Jain, 2003). Organotypic endothelial-vSMC co-culture models demonstrate that paracrine mural cell-derived VEGF is crucial to endothelial capillary-network-like formation and that mural cell Ang-1 regulates endothelial responsiveness to tissue-derived VEGF (Evensen et al., 2010, Korff et al., 2001). This switch from tissue-derived to mural cell-derived VEGF likely promotes vessel maturation, ultimately leading to VEGF-independence and reduced vessel plasticity (Benjamin et al., 1998, Darland and D'Amore, 2001). Importantly, recent studies show that dysregulated tissue VEGF levels can affect mural cell functions and inhibit vessel maturation (Greenberg et al., 2008).

Several previous studies have reported that mural cell types enhance the stability of endothelial cells and formation of functional vessels in tissue implants (Au et al., 2008, Koike et al., 2004, Melero-Martin et al., 2007, Shepherd et al., 2009). Congruently, we demonstrate that the efficiency of intra-scaffold microvascular formation was enhanced by the presence vascular smooth muscle cells. Indeed, a 1:4 EC-mural cell ratio of vascular progenitor cells also generated the greatest vessel density within Matrigel implants (Melero-Martin et al., 2008) A further critical role of peri-vascular cells is to enforce diametral uniformity in branched microvascular networks (Evensen et al., 2009, Gerhardt and Betsholtz, 2003). Genetic and pharmacological inhibition of mural cell recruitment to growing vessels and is associated with exacerbated angiogenesis and endothelial hypertrophy that form irregular, enlarged vessels and aneurysms (Hellstrom et al., 2001, Wilkinson-Berka et al., 2004). Mural cells exert vessel morphogenic control both via modulating endothelial cell signaling responses and contractile vasoconstriction that collectively regulate hemodynamic parameters (Gaengel et al., 2009, Gerhardt and Betsholtz, 2003). Thus to study vascularization in the tissue engineering setting, it is important to employ imaging approaches to facilitate interrogation of the perfused microvascular branched network architecture (Au et al., 2008, McDonald and Choyke, 2003, Sanz et al., 2008). To address this aspect, we utilized functional multiphoton microscopy to selectively image the engineered microcirculation. The acquisition of multiple, stacked images from functionally-labeled scaffold-implants facilitates imaged–based 3D reconstruction and quanitification of spatial peri-vessel cellular relationships. Analysis of 3D-image reconstructions demonstrated that hPASMC preferentially co-localized with perfused vessels. This is congruent with a previous study where intra-vital multiphoton microscopy through cranial windows showed that co-implanted mesenchymal stem cells acquired smooth muscle cell traits and preferentially co-localized with perfused HUVEC (Au et al., 2008). Together, these results highlight the requisite role of proper spatial mural – endothelial cell interactions in achieving a vascularised tissue engineering implant.

Earlier studies have demonstrated that increasing local concentrations of VEGF in ischemic tissues correlated with increased vessel density but did not predict improved tissue blood flow (Ozawa et al., 2004, von Degenfeld et al., 2006). Instead, uniformity of vessel diameters was the most important predictor of enhanced circulation, emphasizing that vessel density measurements are insufficient predictors of angiogenic efficiency. Using functional multiphotonic image analysis we demonstrated that the microcirculation within hPASMC/ HMVEC implant preferentially comprised highly branched, uniform small caliber vessels (<20 μm). In contrast, a recent study that used Bcl-2-expressing human umbilical cord endothelial cells (HUVEC) seeded in poly(glycolic acid) (PGA) scaffold-supported protein gels found that co-engraftment of hPASMC led to an increase in large caliber (>50 μm) vessels (Shepherd et al., 2009). Hence, various combinations of heterogeneous vascular cells can retain a propensity to form vessels of diverse sizes (Garlanda and Dejana, 1997). These results emphasize the importance of using functional morphometric imaging modalities to interrogate engineered vessels formed by clinically-amenable endothelial and mesenchymal progenitor cells that can acquire a spectrum of differentiated characteristics (Au et al., 2008, Melero-Martin et al., 2008, Melero-Martin et al., 2007).

We conducted our experiments with native, early passage human vascular cells in the context of one of the few FDA-approved (PLLA) tissue engineering scaffolds for medical implantation purposes (Freeman JW, 2007, Yun Chen, 2006). In order to promote initial cell attachment we prepared scaffold implants with Matrigel derived extracellular matrix (ECM) proteins (laminin, collagen IV, entactin and heparin sulphate proteoglycan). Using scanning electron microscopy, we show that vascular cells can productively adhere to the scaffold surface under these conditions. The use of a scaffolding material and extracellular matrix gel provides a biocompatible porous skeleton for cell attachment, and therefore functions as a

temporary ECM for the implanted cells. The combination of PLLA and an ECM protein gel comprises an engineered microenvironment that is optimal for many applications, particularly where resistance to compression or contraction is important, and serves as a model for evaluating new cellular combinations for tissue development (Shepherd et al., 2009).

In a recent study, we applied these concepts to develop a tissue engineering-based tumor model to enable evaluation of tumor-vasculature interactions (Gjerdrum et al., 2010). Tri-cellular tumor implants comprising human breast carcinoma, primary microvascular endothelial and vascular smooth muscle cells co-seeded into Matrigel-enriched PLLA scaffolds formed highly vascularized tumors. Interestingly, the presence of a functional engineered microvasculature at two weeks post-implantation corresponded with enhanced tumor growth rate. However, in contrast to the present study, only large caliber diameter vessels were formed (>80 μm). These results exemplify how tissue engineering approaches developed for regenerative medicine applications, afford new opportunities to improve models of disease.

5. Conclusion

The efficient self-assembly of a functional microvasculature in an *in vivo* tissue engineering context from individual vascular components defines a conceptual basis for improving contemporary tissue engineering approaches. The combination of immunohistochemical, flow cytometric and multiphotonic image analysis provides a methodological foundation for improved evaluation of vascular parameters in bioengineered tissues.

Supplementary Material

Refer to Web version on PubMed Central for supplementary material.

Acknowledgments

References

Adams RH, Alitalo K. Molecular regulation of angiogenesis and lymphangiogenesis. Nat Rev Mol Cell Biol. 2007; 8:464–78. [PubMed: 17522591]

Alajati A, Laib AM, Weber H, Boos AM, Bartol A, Ikenberg K, Korff T, Zentgraf H, Obodozie C, Graeser R, Christian S, Finkenzeller G, Stark GB, Heroult M, Augustin HG. Spheroid-based engineering of a human vasculature in mice. Nat Methods. 2008; 5:439–45. [PubMed: 18391960]

Au P, Tam J, Fukumura D, Jain RK. Bone marrow-derived mesenchymal stem cells facilitate engineering of long-lasting functional vasculature. Blood. 2008; 111:4551–8. [PubMed: 18256324]

Beck L Jr, D'amore PA. Vascular development: cellular and molecular regulation. FASEB J. 1997; 11:365–73. [PubMed: 9141503]

Benjamin LE, Hemo I, Keshet E. A plasticity window for blood vessel remodelling is defined by pericyte coverage of the preformed endothelial network and is regulated by PDGF-B and VEGF. Development. 1998; 125:1591–8. [PubMed: 9521897]

Black AF, Berthod F, L'heureux N, Germain L, Auger FA. In vitro reconstruction of a human capillary-like network in a tissue-engineered skin equivalent. FASEB J. 1998; 12:1331–40. [PubMed: 9761776]

Black AF, Hudon V, Damour O, Germain L, Auger FA. A novel approach for studying angiogenesis: a human skin equivalent with a capillary-like network. Cell Biol Toxicol. 1999; 15:81–90. [PubMed: 10408355]

Carmeliet P. Angiogenesis in health and disease. Nat Med. 2003; 9:653–60. [PubMed: 12778163]

Darland DC, D'amore PA. Blood vessel maturation: vascular development comes of age. J Clin Invest. 1999; 103:157–8. [PubMed: 9916126]

Darland DC, D'amore PA. Cell-cell interactions in vascular development. Curr Top Dev Biol. 2001; 52:107–49. [PubMed: 11529428]

Davis GE, Senger DR. Endothelial extracellular matrix: biosynthesis, remodeling, and functions during vascular morphogenesis and neovessel stabilization. Circ Res. 2005; 97:1093–107. [PubMed: 16306453]

Evensen L, Micklem DR, Blois A, Berge SV, Aarsaether N, Littlewood-Evans A, Wood J, Lorens JB. Mural cell associated VEGF is required for organotypic vessel formation. PLoS One. 2009; 4:e5798. [PubMed: 19495422]

Evensen L, Micklem DR, Link W, Lorens JB. A novel imaging-based high-throughput screening approach to anti-angiogenic drug discovery. Cytometry A. 2010; 77:41–51. [PubMed: 19834964]

Freeman Jw WM, Laurencin Ct. Tissue engineering of the anterior cruciate ligament using a braid-twist scaffold design. Journal of biomechanics. 2007; 40:2029–36. [PubMed: 17097666]

Gaengel K, Genove G, Armulik A, Betsholtz C. Endothelial-mural cell signaling in vascular development and angiogenesis. Arterioscler Thromb Vasc Biol. 2009; 29:630–8. [PubMed: 19164813]

Garlanda C, Dejana E. Heterogeneity of endothelial cells. Specific markers. Arterioscler Thromb Vasc Biol. 1997; 17:1193–202. [PubMed: 9261246]

Gerhardt H, Betsholtz C. Endothelial-pericyte interactions in angiogenesis. Cell Tissue Res. 2003; 314:15–23. [PubMed: 12883993]

Gjerdrum C, Tiron C, Hoiby T, Stefansson I, Haugen H, Sandal T, Collett K, Li S, Mccormack E, Gjertsen BT, Micklem DR, Akslen LA, Glackin C, Lorens JB. Axl is an essential epithelial-to-mesenchymal transition-induced regulator of breast cancer metastasis and patient survival. Proc Natl Acad Sci U S A. 2010; 107:1124–9. [PubMed: 20080645]

Gray, H.; WP; Bannister, Lh; Dyson, M.; Collins, P.; Ferguson, Mwj, et al. Gray's Anatomy: The Anatomical Basis of Medicine and Surgery. Churchill-Livingstone; 2004.

Greenberg JI, Shields DJ, Barillas SG, Acevedo LM, Murphy E, Huang J, Scheppke L, Stockmann C, Johnson RS, Angle N, Cheresh DA. A role for VEGF as a negative regulator of pericyte function and vessel maturation. Nature. 2008; 456:809–13. [PubMed: 18997771]

Hall AP. Review of the pericyte during angiogenesis and its role in cancer and diabetic retinopathy. Toxicol Pathol. 2006; 34:763–75. [PubMed: 17162534]

Hellstrom M, Gerhardt H, Kalen M, Li X, Eriksson U, Wolburg H, Betsholtz C. Lack of pericytes leads to endothelial hyperplasia and abnormal vascular morphogenesis. J Cell Biol. 2001; 153:543–53. [PubMed: 11331305]

Holland SJ, Powell MJ, Franci C, Chan EW, Friera AM, Atchison RE, Mclaughlin J, Swift SE, Pali ES, Yam G, Wong S, Lasaga J, Shen MR, Yu S, Xu W, Hitoshi Y, Bogenberger J, Nor JE, Payan DG, Lorens JB. Multiple roles for the receptor tyrosine kinase axl in tumor formation. Cancer Res. 2005; 65:9294–303. [PubMed: 16230391]

Jain RK. Molecular regulation of vessel maturation. Nat Med. 2003; 9:685–93. [PubMed: 12778167]

Jenkins Gw, KC.; Tortora, G. Anatomy and Physiology. John Wiley and Sons; 2007.

Kaully T, Kaufman-Francis K, Lesman A, Levenberg S. Vascularization-The Conduit to Viable Engineered Tissues. Tissue Eng Part B Rev. 2009

Koike N, Fukumura D, Gralla O, Au P, Schechner JS, Jain RK. Tissue engineering: creation of long-lasting blood vessels. Nature. 2004; 428:138–9. [PubMed: 15014486]

Korff T, Kimmina S, Martiny-Baron G, Augustin HG. Blood vessel maturation in a 3-dimensional spheroidal coculture model: direct contact with smooth muscle cells regulates endothelial cell quiescence and abrogates VEGF responsiveness. Faseb J. 2001; 15:447–57. [PubMed: 11156960]

Kutcher ME, Herman IM. The pericyte: cellular regulator of microvascular blood flow. Microvasc Res. 2009; 77:235–46. [PubMed: 19323975]

Lazarous DF, Shou M, Scheinowitz M, Hodge E, Thirumurti V, Kitsiou AN, Stiber JA, Lobo AD, Hunsberger S, Guetta E, Epstein SE, Unger EF. Comparative effects of basic fibroblast growth factor and vascular endothelial growth factor on coronary collateral development and the arterial response to injury. Circulation. 1996; 94:1074–82. [PubMed: 8790049]

Mcdonald DM, Choyke PL. Imaging of angiogenesis: from microscope to clinic. Nat Med. 2003; 9:713–25. [PubMed: 12778170]

Melero-Martin JM, De Obaldia ME, Kang SY, Khan ZA, Yuan L, Oettgen P, Bischoff J. Engineering robust and functional vascular networks in vivo with human adult and cord blood-derived progenitor cells. Circ Res. 2008; 103:194–202. [PubMed: 18556575]

Melero-Martin JM, Khan ZA, Picard A, Wu X, Paruchuri S, Bischoff J. In vivo vasculogenic potential of human blood-derived endothelial progenitor cells. Blood. 2007; 109:4761–8. [PubMed: 17327403]

Muschler GF, Nakamoto C, Griffith LG. Engineering principles of clinical cell-based tissue engineering. J Bone Joint Surg Am. 2004; 86-A:1541–58. [PubMed: 15252108]

Nguyen LL, D'amore PA. Cellular interactions in vascular growth and differentiation. Int Rev Cytol. 2001; 204:1–48. [PubMed: 11243594]

Nor JE, Peters MC, Christensen JB, Sutorik MM, Linn S, Khan MK, Addison CL, Mooney DJ, Polverini PJ. Engineering and characterization of functional human microvessels in immunodeficient mice. Lab Invest. 2001; 81:453–63. [PubMed: 11304564]

Ohnuma K, Yomo T, Asashima M, Kaneko K. Sorting of cells of the same size, shape, and cell cycle stage for a single cell level assay without staining. BMC Cell Biol. 2006; 7:25. [PubMed: 16790072]

Ozawa CR, Banfi A, Glazer NL, Thurston G, Springer ML, Kraft PE, Mcdonald DM, Blau HM. Microenvironmental VEGF concentration, not total dose, determines a threshold between normal and aberrant angiogenesis. J Clin Invest. 2004; 113:516–27. [PubMed: 14966561]

Patterson TE, Kumagai K, Griffith L, Muschler GF. Cellular strategies for enhancement of fracture repair. J Bone Joint Surg Am. 2008; 90(Suppl 1):111–9. [PubMed: 18292365]

Rasband, WS. USNIO. HEALTH. Bethesda, Maryland, USA: 1997–2008. Image J.

Sanz L, Santos-Valle P, Alonso-Camino V, Salas C, Serrano A, Vicario JL, Cuesta AM, Compte M, Sanchez-Martin D, Alvarez-Vallina L. Long-term in vivo imaging of human angiogenesis: critical role of bone marrow-derived mesenchymal stem cells for the generation of durable blood vessels. Microvasc Res. 2008; 75:308–14. [PubMed: 18252255]

Schechner JS, Nath AK, Zheng L, Kluger MS, Hughes CC, Sierra-Honigmann MR, Lorber MI, Tellides G, Kashgarian M, Bothwell AL, Pober JS. In vivo formation of complex microvessels lined by human endothelial cells in an immunodeficient mouse. Proc Natl Acad Sci U S A. 2000; 97:9191–6. [PubMed: 10890921]

Shepherd BR, Jay SM, Saltzman WM, Tellides G, Pober JS. Human aortic smooth muscle cells promote arteriole formation by coengrafted endothelial cells. Tissue Eng Part A. 2009; 15:165–73. [PubMed: 18620481]

Silverthorn Du, OW.; Garrison, Cw; Silverthorn, Ac; Johnson, Br. Human Physiology -An Integrated Approach. San Fransisco:

Silverthorn, DU.; William, CO.; Garrison, CW.; Silverthorn, AC.; Johnson, BR. Human Physiology - An Integrated Approach. San Fransisco: Daryl Fox; 2004.

Swift S, Lorens J, Achacoso P, Nolan GP. Rapid Production of Retroviruses for Efficient Gene Delivery to Mammalian Cells Using 293T Cell-Based Systems. Current Protocols in Immunology. 1999:10.17.14–10.17.29.

Von Degenfeld G, Banfi A, Springer ML, Wagner RA, Jacobi J, Ozawa CR, Merchant MJ, Cooke JP, Blau HM. Microenvironmental VEGF distribution is critical for stable and functional vessel growth in ischemia. FASEB J. 2006; 20:2657–9. [PubMed: 17095533]

Wenger A, Kowalewski N, Stahl A, Mehlhorn AT, Schmal H, Stark GB, Finkenzeller G. Development and characterization of a spheroidal coculture model of endothelial cells and fibroblasts for

improving angiogenesis in tissue engineering. Cells Tissues Organs. 2005; 181:80–8. [PubMed: 16534202]

Wilkinson-Berka JL, Babic S, De Gooyer T, Stitt AW, Jaworski K, Ong LG, Kelly DJ, Gilbert RE. Inhibition of platelet-derived growth factor promotes pericyte loss and angiogenesis in ischemic retinopathy. Am J Pathol. 2004; 164:1263–73. [PubMed: 15039215]

Yun Chen AFTM, Wang Min, Jiashen Li, Wong MS. PLLA scaffolds with biomimetic apatite coating and biomimetic apatite/collagen composite coating to enhance osteoblast-like cells attachment and activity [Online]. 2006
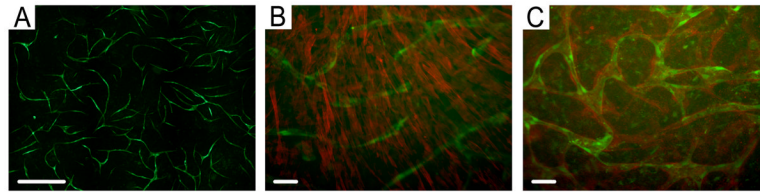
Figure 1. HMVEC and hPASMC form capillary-like networks in vitro
(**A**) Live cell fluorescence microscopy imaging of a capillary-like network formed by GFP-expressing HMVEC cells after 5 days in co-culture (1:4) with hPASMC (*unlabeled*). (**B**) Localization of hPASMC (α-SMC actin, *red*) in a 5 day co-culture with GFP-HMVEC (*green*). (**C**) Fluorescence microscopy analysis of peri-endothelial Collagen XVIII-deposition (red) in GFP-HMVEC (*green*) – hPASMC (*unlabeled*) 5 day co-culture. Scale bar: 50 μm.

Page 14
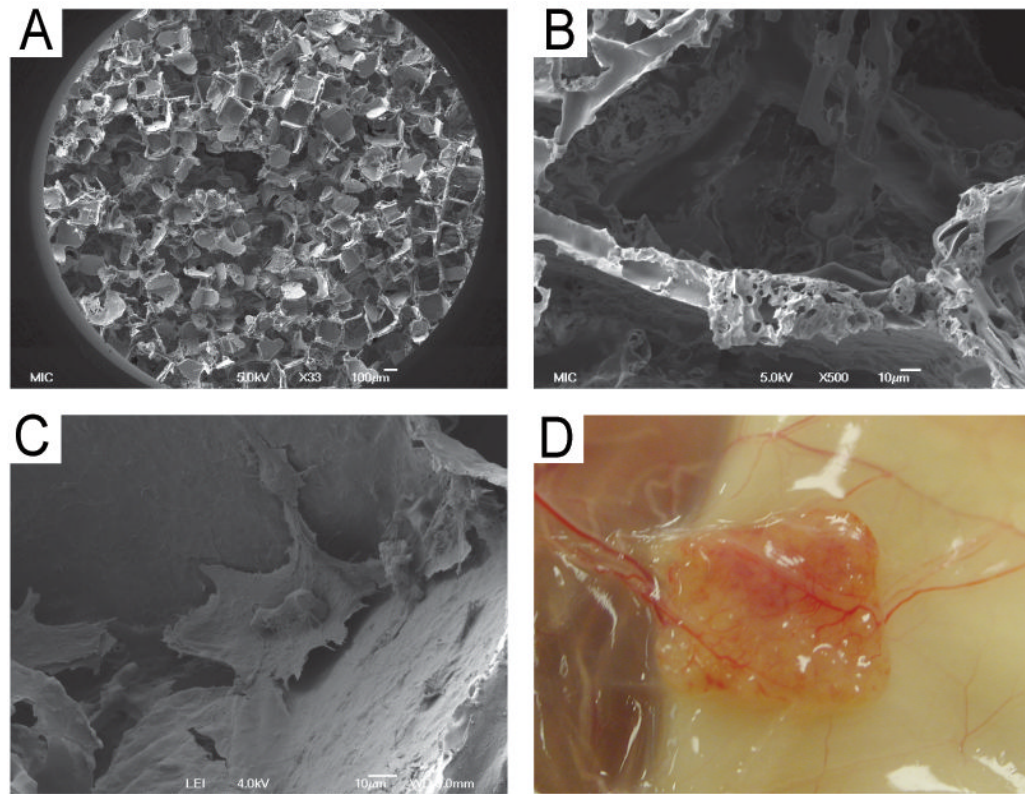
Figure 2. PLLA scaffolds support cell attachment
Biocompatible and biodegradable Poly L-lactic Acid (PLLA) scaffolds, produced by a
solvent-casting particulate-leaching technique, have a highly porous structure with an
average pore size of 400 μm. Scanning electron microscope images 33x (**A**) and 500x (**B**)
show the deep pores penetrating the scaffold. (**C**) PLLA scaffolds support cell attachment as
illustrated by a primary human vascular smooth muscle cell attaching to the wall of a
scaffold pore. (**D**) A subcutaneous PLLA scaffold seeded with human vascular cells 14 days
post-implantation.
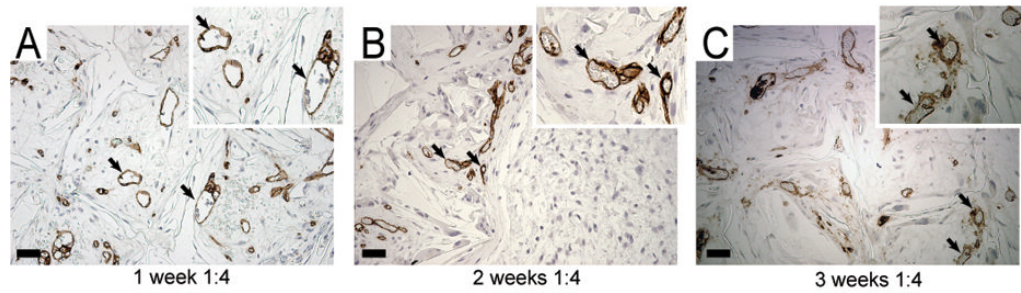
Figure 3. Morphological and immunohistological analysis of scaffold microvasculature development
Scaffold implants were excised at different timepoints and embedded in paraffin. Tissue sections were stained with anti-human CD31 (*brown*) and haematoxylin. Longitudinal analysis of CD31-staining human microvessels formed within scaffolds seeded with HMVEC and hPASMC (1:4) at (**A**) 7 days, (**B**) 14 days and (**C**) 21 days post-implantation. The presence of intralumenal red blood cells within patent anti-CD31 stained vessels demonstrates that the engineered human microvessels are functional and perfused by the host blood circulation (*arrows*, *inset*). Scale bar: 50μm.
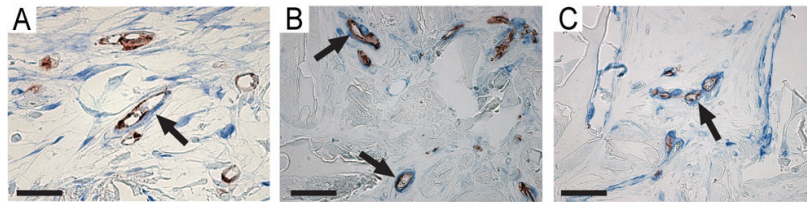
**Figure 4. Co-seeded smooth muscle cells are peri-vascular localized**
Anti-α-smooth muscle cell actin (α-SMA) stained human hPASMC (*blue*) are co-localized with anti-CD31 stained (*brown*) microvessels in HMVEC/hPASMC (1:4) scaffolds 7 days post-implantation (**A**). hPASMC show increased peri-vascular localization in 14 day (B) and 21 day (C) scaffolds. Scale bar: 50μm.
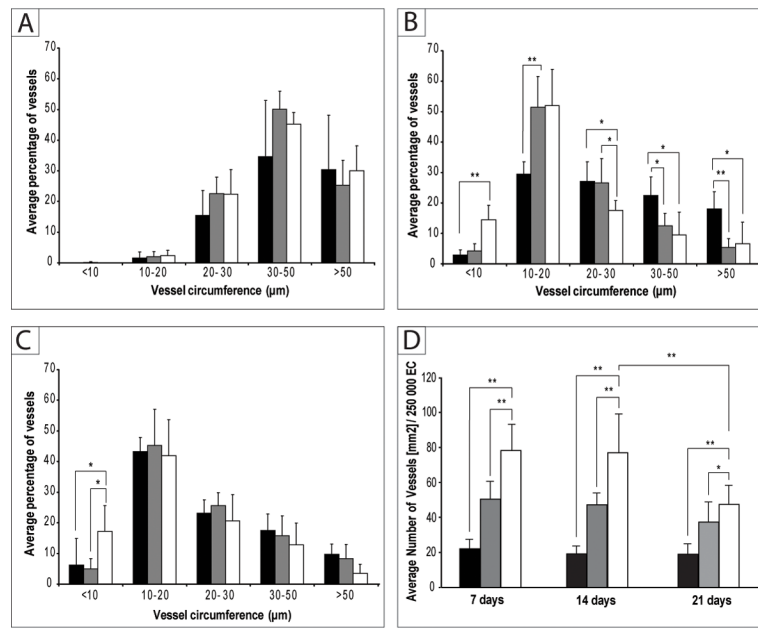
**Figure 5. Smooth muscle cells enhance vessel maturation**
Morphometric analysis of CD31-staining human microvessels formed in scaffolds seeded with HMVEC only (*black bars*) or HMVEC-hPASMC (1:1) (*grey bars*) and HMVEC-hPASMC (1:4) (*white bars*) at 7 days post-implantation (**A**) show a predominance of 30–50 μm diameter vessels indicative of a maturing vasculature. After 14 days (**B**) the CD31-staining human microvessels decreased in caliber. The HMVEC-hPASMC derived microvessels were mainly 10–20 μm in diameter representing a mature microvasculature. HMVEC alone remained distributed among larger caliber microvessels. After 21 days (**C**), the microvessels in all the scaffolds are predominately 10–20 μm in diameter. The 1:4 HMVEC-hPASMC displayed a much larger percentage of small caliber vessels. (**D**) The efficiency of microvascular formation (microvascular density per 250 000 HMVEC) was enhanced by the presence of hPASMC. * $p < 0.05$, ** $p < 0.01$.
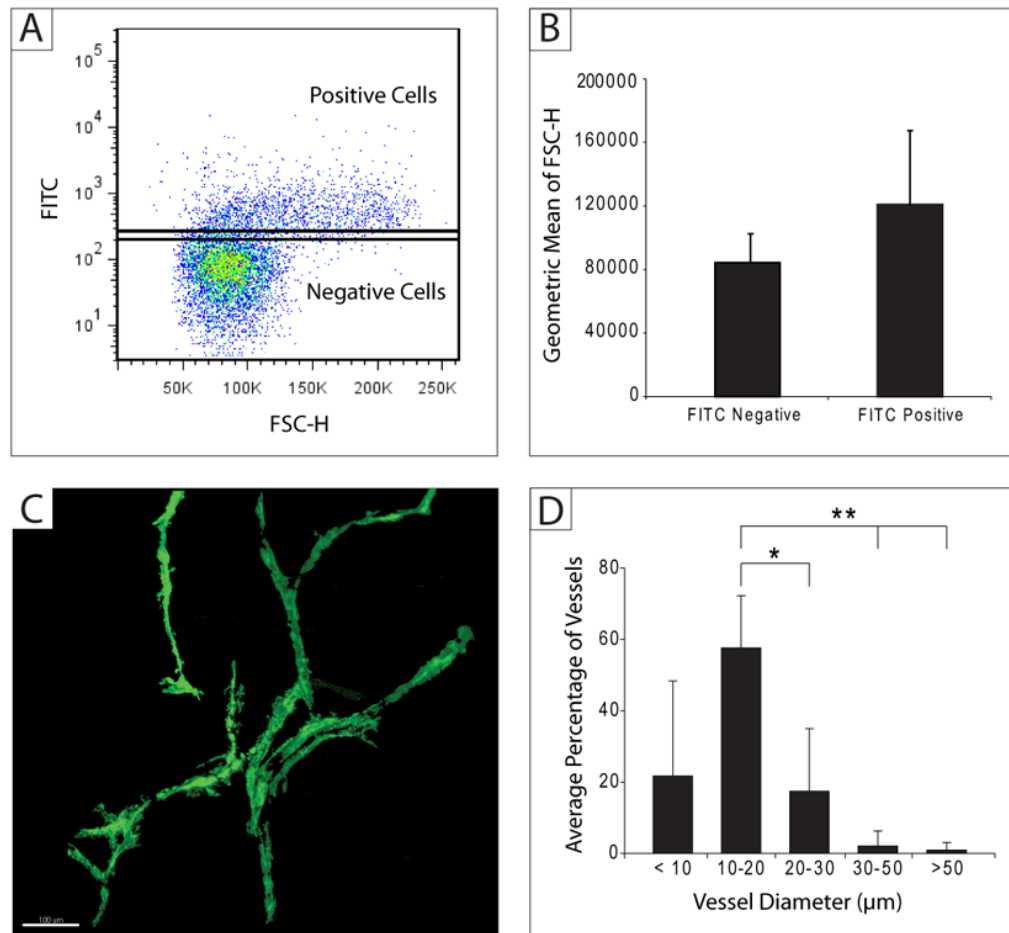
Figure 6. Functional analysis of scaffold microcirculation by fluorescence angiography
Animals were injected at 14 days post-implantation with UEA-Lectin-FITC 30 minutes prior
to scaffold recovery to selectively label perfused human endothelial cells. (**A**) Bivariate flow
cytometry analysis of cells harvested from scaffolds. UEA-Lectin-FITC fluorescence-
positive cells (*upper box*) correlated with higher forward light scatter (FSC) relative to non-
staining cells (*lower box*). (**B**) Mean forward light scatter (FSC) values of perfused UEA-
Lectin-FITC fluorescence-positive HMVEC cells versus non-staining cells. (**C**) Multiphoton
fluorescence microscopy image analysis (IMARIS) of perfusion-labeled UEA-1-lectin-FITC
human microvasculature within a 14-day scaffold shows extensive branching of uniform
microvessels. (**D**) Morphometric analysis of UEA1-lectin-FITC stained human microvessels
from 4 independent experiments shows that functional microvessels are predominately 10–
20 μm in diameter.
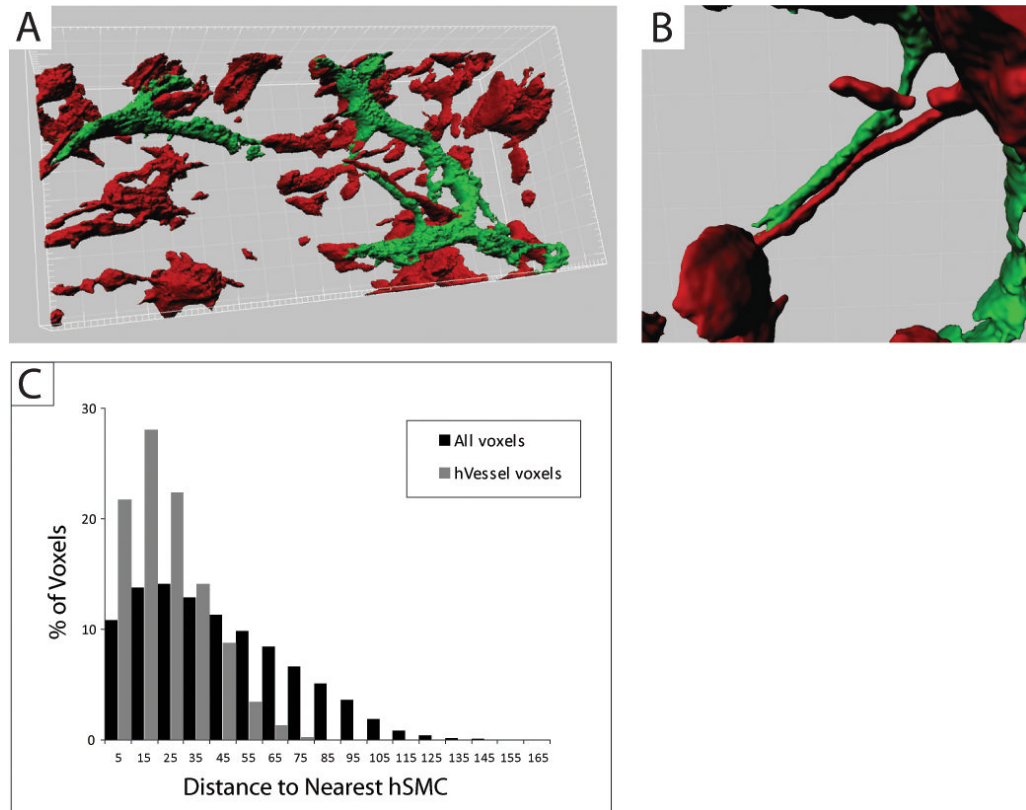
Figure 7. Perfused vessels preferentially co-localize with smooth muscle cells within scaffold
(**A**) Multiphoton fluorescence microscopy 3D-image analysis (IMARIS) of RFP-expressing hPASMC and UEA1-lectin-FITC stained human microvessels within a 14 day scaffold. (**B**) Implanted RFP-expressing hPASMC are frequently peri-vascular localized. (**C**) Distribution of distances (determined by Euclidean Distance Transformation) to the nearest hPASMC/ RFP (*red voxel*) from functional UEA-1-lectin-FITC stained human microvessels (*green voxel*) and all voxels within the 3D-image. The measured mean distance between perfused vessels and hPASMC (22.6 ± 14.6 μm) is significantly smaller than would be expected for randomly distributed vessels (43.1 ± 0.07 μm); $p < 0.00001$.